Absolute excited state absorption cross section measurements in Er^{3+}:$LiYF_4$ for laser applications around 2.8 μm and 551 nm

2000 J. Phys.: Condens. Matter 12 6943

(http://iopscience.iop.org/0953-8984/12/30/322)

J. Phys.: Condens. Matter **12** (2000) 6943–6957. Printed in the UK PII: S0953-8984(00)12400-2

Absolute excited state absorption cross section measurements in Er^{3+}:$LiYF_4$ for laser applications around 2.8 μm and 551 nm

C Labbé, J-L Doualan, S Girard, R Moncorgé and M Thuau

Centre Interdisciplinaries de Recherche Ions Lasers, UMR 6637, CEA–CNRS–ISMRA, Université de Caen, 6 Boulevard Maréchal Juin, 14 050 Caen Cédex, France

E-mail: doualan@spalp255.ismra.fr

Received 7 March 2000

Abstract. Using a pump–probe technique, absolute excited state absorption cross sections are measured in various Er^{3+} doped laser crystals in a wavelength domain extending from 0.53 to 2.9 μm. The gain cross section around 2.8 μm and the population ratio between the involved levels $^4I_{11/2}$ and $^4I_{13/2}$ are measured for different Er^{3+} concentrations and pumping wavelengths. The cross sections for the transitions involved in the upconversion pumping processes of the characteristic green emission of Er:$LiYF_4$ are also estimated and discussed. A comparison is made between these results and those obtained semi-theoretically by using the Judd–Ofelt formalism.

1. Introduction

The erbium doped fluoride crystals present different laser emission wavelengths, of which the most interesting one is around 2.8 μm [1] with the transition $^4I_{11/2} \rightarrow {}^4I_{13/2}$. This laser wavelength is used for medical [2] and LIDAR [3] applications, due to the strong vibrational absorption of water. CW laser emission can be obtained by pumping around 1.51 μm [4], 970 nm [5], 795 nm [1] or 514 nm [6] from the $^4I_{15/2}$ ground state into the $^4I_{13/2}$, $^4I_{11/2}$, $^4I_{9/2}$ or $^4H_{11/2}$ excited states, respectively. At room temperature, another important laser emission wavelength also appears around 550 nm [7] ($^4S_{3/2} \rightarrow {}^4I_{15/2}$). In the CW regime, it can be produced by two-step excited-state absorption (ESA) around 810 nm [8] or 970 nm [9] via the $^4I_{9/2}$ or the $^4I_{11/2}$ level, respectively. This wavelength emission can be also obtained via photon avalanche upconversion [10], which uses different ESA wavelengths in the range between 550 and 750 nm.

Therefore ESA plays a major role in a large wavelength domain and its investigation is necessary to optimize the laser emissions and understand the underlying mechanisms. Energy transfer between ions can be described with the aid of purely spectroscopic microparameters. They are proportional to the spectral overlap between the interacting transitions of the ions. Thus, even for upconversion energy transfer processes ESA transitions are implied. This is the reason why ESA has been studied very carefully in a number of important Er doped laser materials such as YAG, $YAlO_3$ and YVO_4 [11, 12] for oxides and BaY_2F_8, $LiYF_4$ and KYF_4 [11, 13] for fluorides.

Within an ESA experiment, absolute cross sections can be easily obtained after spectrum calibration only in some cases, in particular for most of the oxide materials (YAG, YVO_4, ...).

0953-8984/00/306943+15$30.00

Indeed, in these crystals, there is a high rate of multiphonon relaxation, due to phonons of high energy (600 to 1100 cm^{-1}). Therefore, only the first excited level $^4I_{13/2}$, with a lifetime of a few milliseconds, can be populated efficiently. ESA then almost essentially occurs in this $^4I_{13/2}$ level [11] and calibration of ESA spectra in absolute cross section units becomes relatively easy. In contrast, with fluoride crystals, phonons have lower energies (300 to 600 cm^{-1}) and non-radiative multiphonon relaxations down to the $^4I_{13/2}$ metastable level are less probable. Since both first excited levels $^4I_{13/2}$ and $^4I_{11/2}$ have lifetimes of a few milliseconds, ESA takes place predominantly from these two levels and their population ratio changes with the pumping conditions and the Er^{3+} ion concentration. In these conditions, if the population ratio is not measured during the calibration, only relative ESA cross section values can be obtained [11, 13].

The aim of this work is to describe first an ESA calibration method based on the measurement of this population ratio in the case of Er^{3+} doped fluoride crystals. Then, this method is applied to the case of Er:$LiYF_4$ in a broad spectral domain (0.53 to 2.9 μm). The gain cross sections around 2.8 μm and the population ratio are then obtained for different Er:$LiYF_4$ crystals, which is necessary for a complete laser emission analysis. The upconversion laser emission at 551 nm is also studied by measuring the ESA cross sections of the transitions involved in the two-photon absorption and photon avalanche upconversion processes mentioned above. Our results are then confronted with the literature data and the integrated cross sections and the radiative probabilities deduced from the ESA measurements are compared with those obtained with the aid of the Judd–Ofelt formalism.

2. Experimental considerations

2.1. General conditions

Three single crystals were grown in our laboratory by using the Czochralsky technique, 1.06, 4.75 and 14.75 at.% Er^{3+}:$LiYF_4$, concentrations determined with the aid of the inductively coupled plasma (ICP) method.

ESA spectra were recorded by a pump–probe technique [11] based on two CW light sources, a probe lamp and a pump laser, where each is modulated at different frequency ($\nu_{probe} \approx 1$ kHz and $\nu_{pump} \approx 10$ Hz). Details can be found in [12]. Two lock-in amplifiers placed in series process the signal. The first one, locked at ν_{probe}, gives the mean transmission intensity I through the sample. The second, locked at ν_{pump}, measures the transmission variation ΔI induced by the pump. A computer then acquires the two measured values I and ΔI to provide the ratio $\Delta I/I$ at each wavelength. To record the spectra around 2.8 μm, the whole experimental setup was placed in a dried box with nitrogen gas circulation to avoid signal perturbations due to water absorption. Moreover CaF_2 lenses were used, for a good transmission in the IR. Polarized measurements were made thanks to a calcite Glan–Thompson polarizing prism. However the calcite transmission dropped near 2.9 μm and therefore it was not adequate, explaining why the signal to noise ratio became so bad beyond this wavelength.

To establish the relationship between the ratio $\Delta I/I$ and the various cross-sections which come into play, we have to consider the intensity of the probe signal, when the pump is off and on. This intensity is then described by the following formula:

$$I_{off}(\lambda) = I_0\, e^{-\sigma_{GSA} N_T L} \tag{1}$$

$$I_{on}(\lambda) = I_0 \exp\left(-\sigma_{GSA}\left[N_T - \sum_{i=1}^{p} N_i \right] L + \sum_{i}^{p} N_i [\sigma_{SE}^{(i)} - \sigma_{ESA}^{(i)}] L \right) \tag{2}$$

where σ_{GSA}, $\sigma_{SE}^{(i)}$ and $\sigma_{ESA}^{(i)}$ are respectively the cross sections of the ground-state absorption

(GSA), of the stimulated emission (SE) and of the excited-state absorption (ESA) from the populated multiplet (i), N_i the population of multiplet i, N_T the total population density, L is the length of the crystal and I_0 is the incident pump intensity, including the Fresnel reflection on both side and diffusion losses inside the crystal.

By using the same procedure and approximations used in [12], we obtain:

$$\frac{\Delta I}{I}(\lambda) = AL\left[\sigma_{GSA}(\lambda)\sum_{i=1}^{p} N_i + \sum_{i=1}^{p} N_i[\sigma_{SE}(\lambda)^{(i)} - \sigma_{ESA}(\lambda)^{(i)}]\right] \tag{3}$$

where A is the calibration coefficient of the experiment. Since the $^4I_{13/2}$ and $^4I_{11/2}$ metastable levels can be significantly populated under optical pumping in the erbium doped fluoride crystals (see figure 1), $p = 2$ in the summation of equation (3) and

$$\frac{\Delta I}{I}(\lambda) = AL[(N_1 + N_2)\sigma_{GSA}(\lambda) + N_1[\sigma_{SE}(\lambda)^{(1)} - \sigma_{ESA}(\lambda)^{(1)}] + N_2[\sigma_{SE}(\lambda)^{(2)} - \sigma_{ESA}(\lambda)^{(2)}] \tag{4}$$

where N_1 and N_2 are the populations of the $^4I_{13/2}$ and $^4I_{11/2}$ multiplets, respectively. Stimulated emissions and excited state absorptions starting from the other levels were neglected. Equation (4) then can be transformed to give

$$\frac{\Delta I}{I}(\lambda)A' = \sigma_{GSA}(\lambda) + (1-\beta)[\sigma_{SE}(\lambda)^{(1)} - \sigma_{ESA}(\lambda)^{(1)}] + \beta[\sigma_{SE}(\lambda)^{(2)} - \sigma_{ESA}(\lambda)^{(2)}] \tag{5}$$

where A' is equal to $1/AL(N_1 + N_2)$ and β is the population ratio:

$$\beta = \frac{N_2}{N_1 + N_2}. \tag{6}$$

In the course of calibration, the emission and the ground-state absorption spectra were subtracted from the registered excited-state 'absorption difference' spectra. Therefore, to keep the same spectral resolution for all these spectra, the ground-state absorption and emission spectra were recorded with the same experimental set-up as for the ESA measurements.

2.2. Calibration technique for ESA spectra

The method used to calibrate the ESA spectra when the two levels $^4I_{13/2}$ and $^4I_{11/2}$ are populated proceeds as follows.

(1) The sample transmission $\Delta I/I$ is measured first around 1.5 and 2.8 μm.
Around 1.5 μm there is no SE and ESA starting from $^4I_{11/2}$. Therefore equation (5) can be simplified noticeably:

$$\frac{\Delta I}{I}(\lambda)A' = \sigma_{GSA}(\lambda) + (1-\beta)(\sigma_{SE}(\lambda)^{(1)} - \sigma_{ESA}(\lambda)^{(1)}). \tag{7}$$

The ESA transition $^4I_{13/2} \rightarrow {}^4I_{9/2}$ only weakly overlaps with the $^4I_{15/2} \leftrightarrow {}^4I_{13/2}$ GSA and SE transitions. The calibration then can be done in the short wavelength portion where there is no ESA ($\sigma_{ESA}^{(1)}(\lambda) = 0$). But, the A' parameter and the population ratio β remain undetermined.

(2) An emission spectrum $I(\lambda)$ is thus registered around 2.8 μm by pumping at 970 nm into the $^4I_{11/2}$ level. A partial calibration is obtained by using the so-called Füchtbauer–Ladenburg formula [14], derived from the famous McCumber expression [15]:

$$\sigma_{SE}^{FL}(\lambda) = \frac{\beta_{Rad}}{\tau_{Rad}}\frac{3}{8\pi n^2 c}\lambda^5 I(\lambda)\left(\int \sum_{p=X,Y,Z} \lambda I^P(\lambda)\,\mathrm{d}\lambda\right)^{-1} \tag{8}$$

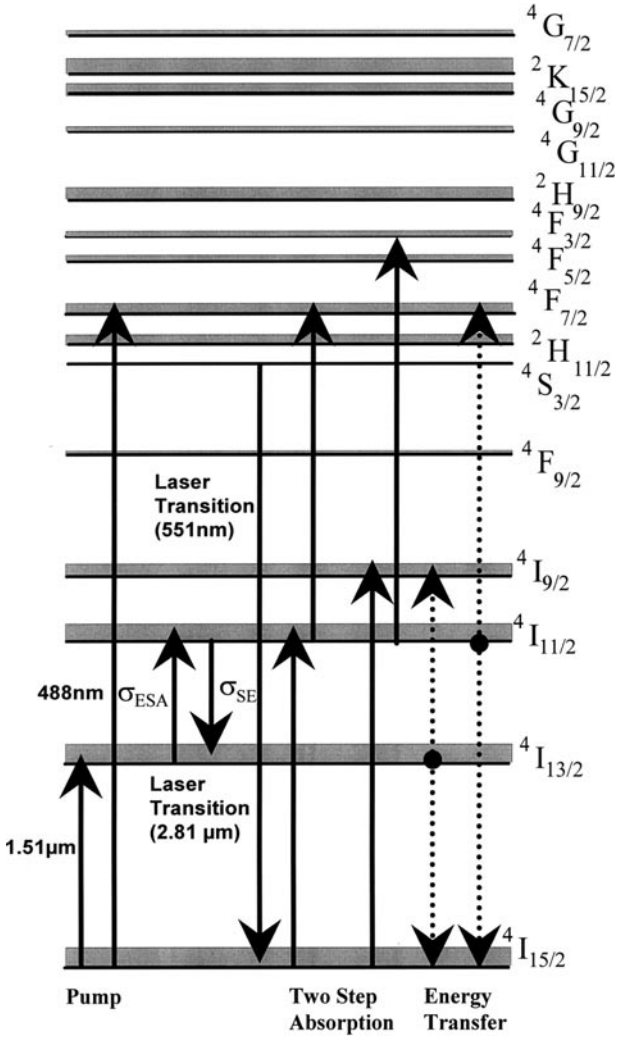

Figure 1. Energy level scheme and main transitions and energy transfer processes involved for the 551 nm and 2.8 μm laser transition in Er:$LiYF_4$.

where β_{Rad} and τ_{Rad} are respectively the radiative branching ratio ($^4I_{11/2} \rightarrow {}^4I_{13/2}$) and radiative lifetime from the $^4I_{11/2}$ level. By taking $I^X = I^Y = I^\sigma$ and $I^Z = I^\pi$ for an uniaxial crystal such as $LiYF_4$, the ESA cross section $\sigma_{ESA}(\lambda)$ is derived by using another well known expression obtained from the reciprocity relation between the Einstein coefficients [15].

$$\sigma_{SE}(\lambda) = \sigma_{ESA}(\lambda)\frac{Z_l}{Z_u}\exp\left(\frac{hc}{kT}\left(\frac{1}{\lambda_{ZL}} - \frac{1}{\lambda}\right)\right) \tag{9}$$

where Z_u and Z_l are the partition functions for the upper and lower multiplets, respectively, and λ_{ZL} is the so-called zero-line wavelength of the transition between the lower Stark levels of these multiplets.

(3) β is then found by adjusting the resulting shape of the linear combination of $\sigma_{SE}(\lambda)^{(2)}$ and $\sigma_{ESA}(\lambda)^{(1)}$ with the $(\Delta I/I)(\lambda)$ spectrum recorded around 2.8 μm, according to the

expression:

$$\frac{\Delta I}{I}(\lambda)A' = \beta\sigma_{SE}(\lambda)^{(2)} - (1-\beta)\sigma_{ESA}(\lambda)^{(1)} \tag{10}$$

which comes from equation (5) with $\sigma_{GSA} = 0$ around 2.8 μm. For β calculation a relative value of β_{Rad}/τ_{Rad} is used.

(4) Knowing β and returning to equation (7), the parameter A' can be calculated, a parameter which can be employed for any portion of the ESA spectra, provided that nothing is changed in the experimental conditions. This calibration coefficient determined, it becomes possible with (8), (9) and (10) to give the absolute value for the radiative probability β_{Rad}/τ_{Rad} and for the cross sections σ_{SE} and σ_{ESA} of the stimulated emission and ESA transitions $^4I_{11/2} \leftrightarrow {}^4I_{13/2}$.

2.3. Pumping conditions

One possibility is to pump directly into the $^4I_{13/2}$ metastable level to limit the population of the $^4I_{11/2}$ level and to reduce the associated β value to a minimum (figure 1). We used then a home-made colour centre laser (CCL) NaCl:$OH^-(F_2^+)_H$, tunable between 1.48 and 1.70 μm, and the crystal used was the one doped with 1.06 at.% Er^{3+}. Under these conditions, we still observed a small population of the $^4I_{11/2}$ level with an associated population ratio β of 0.05. Thus, even with a low dopant concentration, upconversion energy transfers occur and a small fraction of the ions are promoted up to the $^4I_{11/2}$ level through the upconversion process. However with a low value of β such as the measurement has determined, we obtain a good estimation of the calibration coefficient A'.

To measure the ESA spectra from $^4I_{11/2}$, this level must be more efficiently populated. Also, according to equation (5), it is more favourable to determine both σ_{ESA} and σ_{SE} to obtain $\beta = 0.5$, conditions for which β is close to $(1-\beta)$. To reach these conditions a strongly concentrated crystal, with 14.75 at.% Er^{3+} and an Ar^+ ion laser (from Spectra Physics) emitting at 488 nm are used (figure 1). In this case, there are about equal populations between the first two excited levels and the $(\Delta I/I)(\lambda)$ signal is stronger. Under these conditions, a β value equal to about 0.48 was found. At the same time, it became easier to calculate the A' calibration coefficient corresponding to these new conditions by using equation (10) and knowing the σ_{SE} and σ_{ESA} cross sections in the 2.8 μm range.

2.4. Measurement uncertainties

Cross section measurements suffer from two types of error. One is due to the reciprocity method, i.e. to the uncertainty on the zero-line position, the partition functions and the subtracted background. This uncertainty is of the order of 10% for all the spectra. The second type of error is directly due to the calibration method. The errors are estimated to be of the order of 15% and 25% when the CCL and Ar^+ ion lasers were used, respectively. Under CCL pumping the β value is very low, which means that only the $^4I_{13/2}$ level is significantly populated and that the level $^4I_{11/2}$ is only very weakly operative. On the other hand, under Ar^+ laser pumping, β was estimated equal to 0.48 and the two levels $^4I_{13/2}$ and $^4I_{11/2}$ have approximately the same populations which means a greater uncertainty in the calibration than previously. In the end, we estimated overall uncertainties to about 25% and 35% when the CCL and the Ar^+ ion lasers were used, respectively.

3. Results and discussion

The polarized ESA spectra recorded in various wavelength domains from 0.53 to 2.9 μm are reported in figures 2 to 9. Around 1.5 and 2.8 μm, the spectra are given in π and σ polarizations, while the others are only reported in π polarization. In addition, the GSA and SE cross section spectra are also reported when they are necessary for the analysis.

Spectral resolution is 1.2 nm around 2.8 μm and 0.5 nm in the other spectral ranges. The maximum intensity is given with a wavelength precision of $\pm$0.4 nm around 2.8 μm and $\pm$0.2 nm for the other wavelength domains. Our experimental set-up allows us to detect $\Delta I/I$ signals as low as 10^{-4} while keeping a very good S/N ratio, which generally results in very good quality spectra. Points are missing around 1.5 μm in the corresponding $\Delta I/I$ spectra (see figure 4) because the detector is saturated by the CCL.

The assignments of the various ESA wavelength domains were made with the aid of [16] which gives most of the Stark levels up to 40 000 cm^{-1}. Domains corresponding to ESA from the $^4I_{11/2}$ and $^4I_{13/2}$ were separated by dotted lines in figures 6 to 9.

The line positions deduced from the transitions between the involved Stark levels fitted well the observed ones.

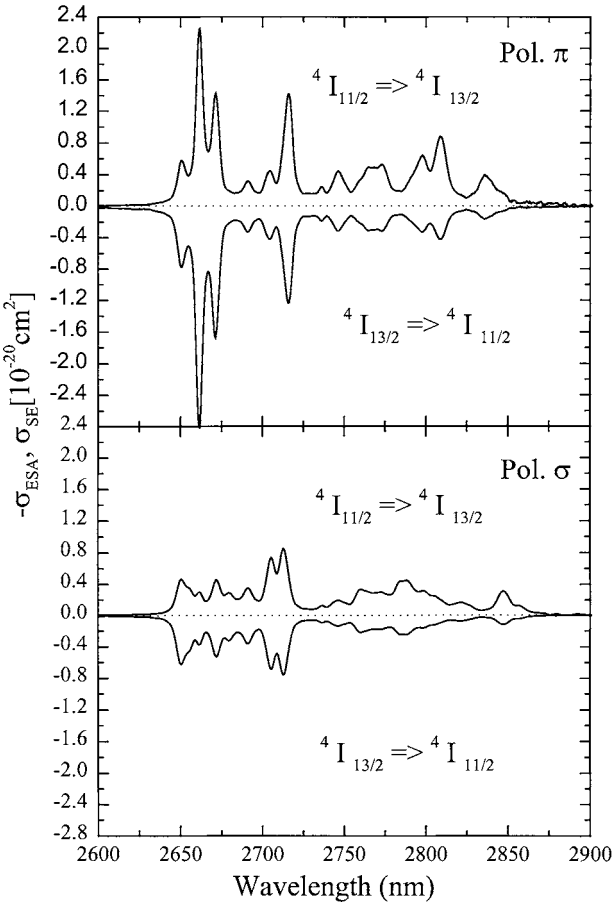

Figure 2. ESA and SE cross sections spectra of Er:$LiYF_4$ around 2.8 μm.

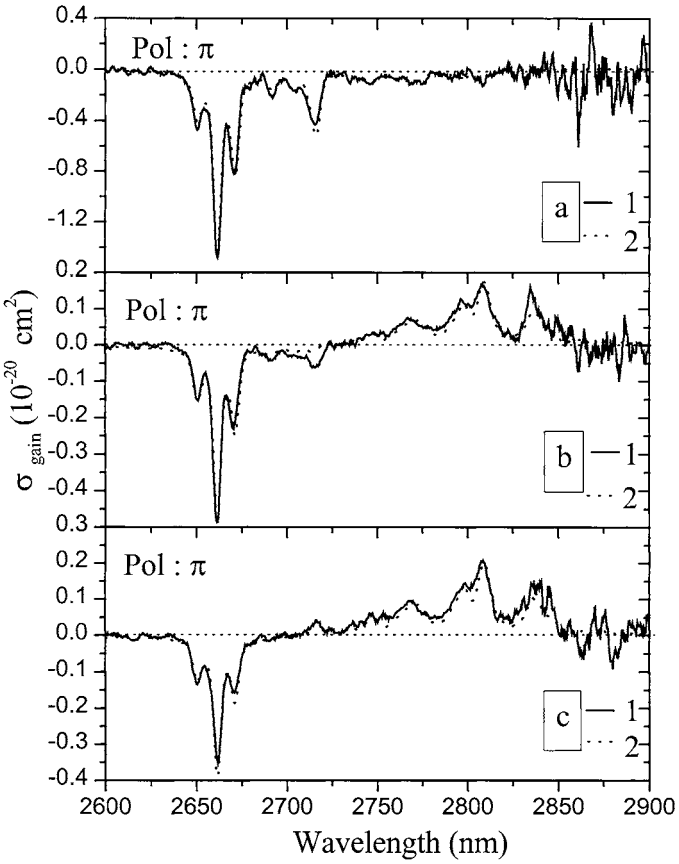

Figure 3. Gain cross section spectra measured (1) and calculated from ESA and SE cross sections (2) of Er:$LiYF_4$ around 2.8 μm for 1.06% (a), 4.75% (b) and 14.75% (c) Er doped $LiYF_4$, pumping at 488 nm.

3.1. Comparison with the results deduced from the Judd–Ofelt analysis

In the JO formalism [17, 18] the Ω_t parameters ($t = 2, 4, 6$) are determined with the aid of the GSA spectra and give access to the radiative lifetime τ_{Rad} and the branching ratio β_{Rad} of each energy level. Table 1 gives these values for the transition $^4I_{11/2} \rightarrow {}^4I_{13/2}$ along with the corresponding radiative transition probability β_{Rad}/τ_{Rad} as calculated with the Ω_t parameters which can be found in the literature. The table 1 also gathers the experimental value $\beta_{Rad}/\tau_{Rad} = 20\ s^{-1}$ which is found by fitting equation (8) to the 2.8 μm fluorescence spectra. This value is in good agreement with three different literature results [19–21], with a relative difference of less than 13%. The result reported in [22] is probably wrong.

Knowing the Ω_t parameters and the matrix elements which are necessary in the JO analysis, the integrated cross sections of the transitions between all the multiplets can be calculated. This was made for the 1.5 and 2.8 μm spectral ranges by calculating integrals $(\int \sigma_{ESA}\, d\lambda)^{JO}$ and by using equation (14) of [12]. These values can then be compared with those obtained experimentally by calculating integrals $(\int \sigma_{ESA}\, d\lambda)^{Mea}$ based on the calibrated ESA cross section spectra. The respective values are reported in table 2, with their relative differences. The agreements are excellent with only 6.8 and 17.8% uncertainties, which makes us confident both in the JO analysis and in our measurements.

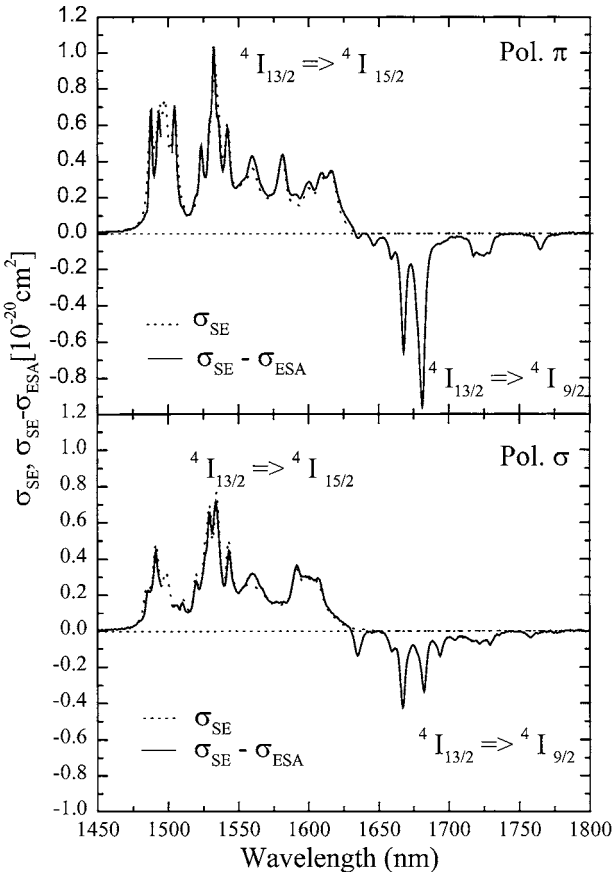

Figure 4. ESA and SE cross section spectra of Er:$LiYF_4$ around 1.6 μm.

Table 1. Comparison of the ratio $(\beta_{Rad}/\tau_{Rad})_{JO}$ and $(\beta_{Rad}/\tau_{Rad})_{Exp}$ from the level $^4I_{11/2}$ derived from a Judd–Ofelt analysis and experimentally for $Er^{3+}LiYF_4$.

Reference	β_{Rad}	τ_{Rad} (ms)	$\left(\frac{\beta_{Rad}}{\tau_{Rad}}\right)_{JO}$ (s^{-1})	$\left(\frac{\beta_{Rad}}{\tau_{Rad}}\right)_{Exp}$ (s^{-1})	Relative difference (%)
[19]	0.15	6.7	22.4		−12
[20][a]	0.17	8.8	19.3	20	3.5
[21]	0.11	6.3	17.46		13
[22]	0.087	8.3	10.5		47

[a] Calculated with the oscillator strengths.

3.2. Results obtained around 2.8 μm

The 2.81 μm emission line with a stimulated emission cross section of about 8.8×10^{-21} cm^2 in π polarization (see figure 2) is probably one of the most interesting laser transitions ($^4I_{11/2} \rightarrow {}^4I_{13/2}$) in this Er^{3+}-doped fluoride, in agreement with the laser results reported in [23]. Our cross section values (table 3), however, are slightly smaller than that reported

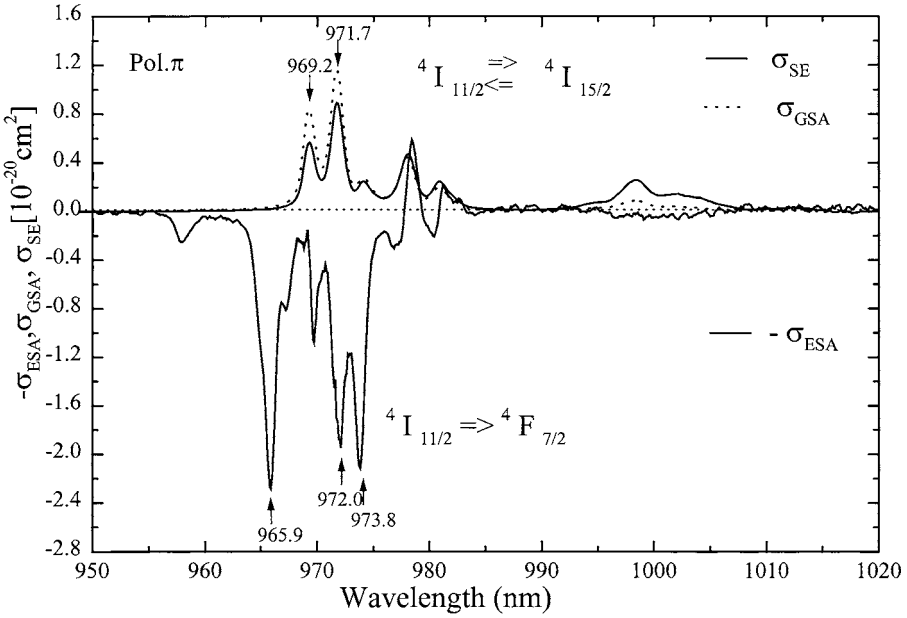

Figure 5. GSA, ESA and SE cross section spectra of Er:$LiYF_4$ around 970 nm.

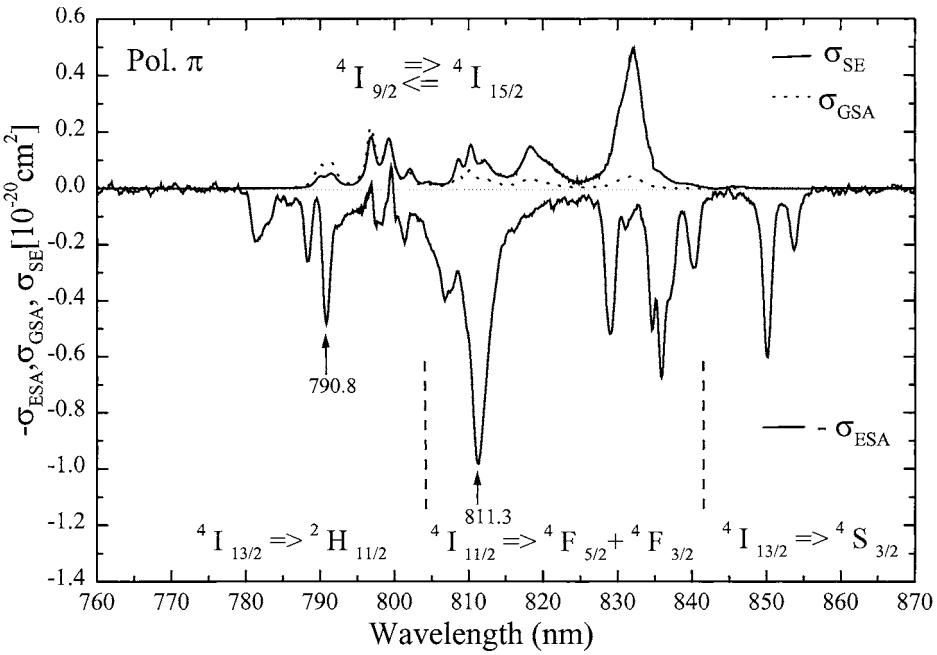

Figure 6. GSA, ESA and SE cross section spectra of Er:$LiYF_4$ around 800 nm.

in the literature [24, 25] but remain very close, except for the emission at 2.661 μm when comparison is made with [24].

Laser transition occurs between two metastable levels $^4I_{11/2}$ and $^4I_{13/2}$ with 7 and 14.6 ms lifetimes, respectively, for a 0.013% Er^{3+} doped $LiYF_4$ [19]. Consequently, CW laser emission

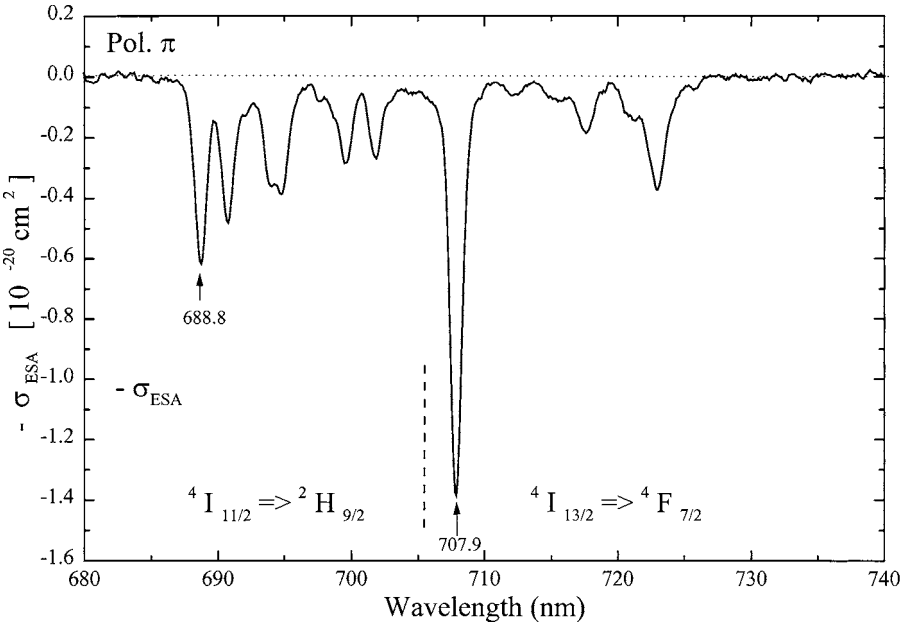

Figure 7. ESA cross section spectra of Er:$LiYF_4$ around 700 nm.

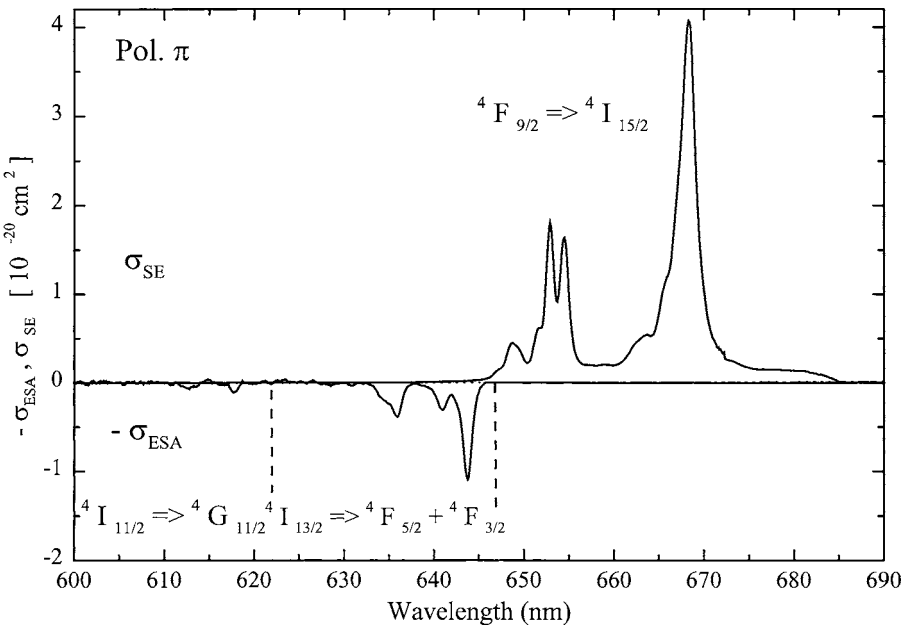

Figure 8. ESA and SE cross section spectra of Er:$LiYF_4$ around 650 nm.

should be greatly reduced or even prevented due to bottlenecking effects (figure 1). CW laser emission, however, could be observed with a very good efficiency of about 50% [23]. This is due to strong upconversion energy transfers ($^4I_{13/2}$, $^4I_{13/2} \rightarrow {}^4I_{9/2}$, $^4I_{15/2}$) which take place starting from the $^4I_{13/2}$ metastable level and depopulate it in favour of higher lying energy

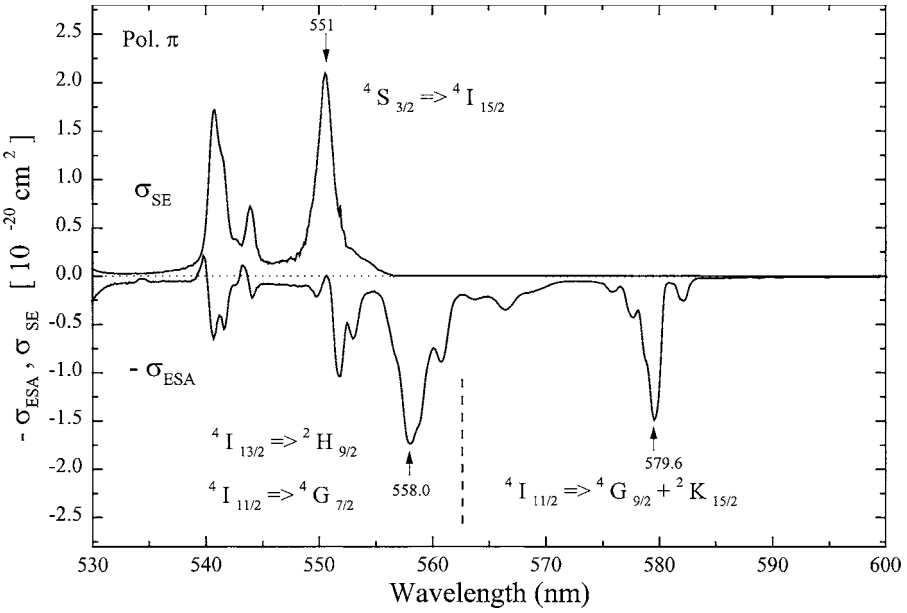

Figure 9. ESA and SE cross section spectra of Er:$LiYF_4$ around 560 nm.

Table 2. Comparison of the integrated ESA cross sections derived from a Judd–Ofelt analysis and measured experimentally.

Range (μm)	Transitions	λ (nm)	$\left(\int \sigma_{ESA}\,d\lambda\right)^{JO}$ (10^{-20} cm^2 nm)	$\left(\int \sigma_{ESA}\,d\lambda\right)^{Mea}$ (10^{-20} cm^2 nm)	Relative difference (%)
2.6–2.9	$^4I_{13/2} \rightarrow {}^4I_{11/2}$	2743	60.13	56.3	−6.8
1.5–1.8	$^4I_{13/2} \rightarrow {}^4I_{9/2}$	1705	13.46	11.43	−17.8

Table 3. $Er^{3+}LiYF_4$ emission cross section results (π polarization) obtained in the 2.8 μm range.

Wavelength (μm)	Reference	$(\sigma_{em})_{lit}$ (10^{-20} cm^2) literature	$(\sigma_{em})_{work}$ (10^{-20} cm^2) this work	Relative difference
2.81	[24] [25]	1.25	0.90	−39
2.715	[24]	1.8	1.41	−28
	[25]	1.75		−24
2.661 (max)	[24]	3.8	2.23 (max)	−70
	[25]	2.1		6

levels, among which, after rapid relaxation, is the $^4I_{11/2}$ laser level itself. Simultaneously, two other important energy transfers must be involved: one involving the $^4I_{11/2}$ laser level ($^4I_{11/2}$, $^4I_{11/2} \rightarrow {}^4S_{3/2}$, $^4I_{15/2}$), which reduces its population, and another one ($^4I_{15/2}$, $^4S_{3/2} \rightarrow {}^4I_{9/2}$, $^4I_{13/2}$), which tends to reequilibrate the populations between the two laser levels, knowing that excitation of level $^4I_{9/2}$ rapidly relaxes down to $^4I_{11/2}$. The corresponding energy transfer parameters depend both on the pump power density and the ion populations in the ground and the excited states. Therefore, it is difficult to determine them with precision and population

Table 4. Population ratio β between levels $^4I_{11/2}$ and $^4I_{13/2}$ found in Er^{3+}:$LiYF_4$ with different erbium concentration at different pump wavelengths.

Wavelength excitation (μm)	Erbium concentration (at.%)		
	1.06	4.75	14.75
0.488	0.27	0.46	0.48
1.51	0.05	0.27	0.42

rate equations must be used very carefully [26]. They cannot be used with a good accuracy, for example, to predict the population ratio β.

Using equation (10) and the calibrated $\Delta I/I$ spectra in the 2.9 μm spectral region, the gain cross section can be directly obtained since:

$$\sigma_g(\lambda) = \beta\sigma_{SE}(\lambda)^{(2)} - (1-\beta)\sigma_{ESA}(\lambda)^{(1)} = A'\frac{\Delta I}{I}(\lambda). \tag{11}$$

At 2.81 μm which is the wavelength of main laser emission in $LiYF_4$ [23], gain will be positive if $\beta > 0.32$. Different ion concentrations and pump wavelength were studied (table 4).

With the low concentration crystal (1.06 at.% Er^{3+}), population inversion is not reached either in the case of 488 nm or in the case of 1.51 μm laser excitation, with β values $\beta = 0.27$ and 0.05, respectively. As a matter of fact, CW laser emission has never been observed, to the best of our knowledge, in a so lightly doped crystal.

Under pumping at 488 nm the population ratio β increases quickly with concentration ($\beta = 0.46$ for 4.75 at.% Er^{3+}) and finally saturates ($\beta = 0.48$ for 14.75 at.% Er^{3+}). The population inversion does not change too much when the dopant concentration is increased beyond 4.75 at.% Er^{3+}. It is interesting to use, however, highly doped crystals just to increase the excited ion density, knowing that laser gain is proportional to the product of the gain cross section by the sum of the excited ion densities in the two excited levels $^4I_{11/2}$ and $^4I_{13/2}$. This is the reason why, according to [27] for example, the laser efficiency was found to increase from about 20 to 30% when the Er^{3+} concentration was increased from 4% to 15%.

Under pumping at 1.51 μm, a 4.75 at.% Er^{3+} concentration is too small to observe laser emission ($\beta = 0.3$). But for 14.75 at.% Er^{3+}, the population ratio rises to 0.42 which is very close to the population inversion observed under pumping at 488 nm. Thus CW laser emission could be observed under pumping at 1.51 μm into the terminal level of the laser transition, a curiosity which was already observed in the case of Er^{3+}:CaF_2 after pumping around 1.51 μm [4, 28]. At an erbium concentration of 14.75 at.%, the gain is maximum at 2.81 μm [23] with a cross section value of 2×10^{-21} cm^2. In spite of this low value the laser emission is observed with a good efficiency due to the strong ion concentration. Other laser wavelengths were already detected in the past at different wavelengths between 2.66 and 2.85 μm [6, 23]. In the cw regime long wavelengths are promoted (see figure 3). In [6], the authors reported the time evolution of these other laser emissions during long pulse pumping. At the beginning of the pump pulse, laser emission occurs at 2.66 μm, which corresponds to the maximum SE cross section (see figure 2). This means the population ratio is close to one. Very quickly, then, the wavelength shifts to 2.71 μm which is the next more intense line in the SE cross section spectrum. In the end, laser emission sets at 2.81 μm. In the CW regime, the laser emission wavelength could be tuned between 2.77 and 2.85 μm.

Finally, it is worth noticing that in our experiments the measured σ_g values correspond in fact to a near-threshold laser regime. During laser emission in the cw regime the product $\sigma_g(N_1 + N_2)$ stays constant to compensate the cavity losses. But the population N_1 and N_2 of the two laser levels can change due to stimulated emission so that the pumping efficiency

could be modified when the pump power is increased. Laser measurements reported in [27] show, however, a linear variation of the slope efficiency which indicates a stabilization of σ_g and level population above threshold. This is in agreement with our observation since, in our experiments, we did not observe any noticeable variation of the gain cross section when the pump power was increased. Population equilibrium between the $^4I_{11/2}$ and $^4I_{13/2}$ levels thus occur in any regime probably because of the great efficiency of the inter-ionic energy transfer mentioned above. In these conditions, our population inversion measurements can be used more directly for the simulation of laser emission than population rate equations [26].

3.3. Results obtained between 0.53 and 1.8 μm

3.3.1. General description. The cross section spectra associated with the ESA transitions from the $^4I_{13/2}$ and $^4I_{11/2}$ metastable levels are reported in figures 4 to 9. In π polarization, for $Er^{3+}LiYF_4$, the results published in the literature [11, 13, 29, 30] were only reported in relative cross section units, i.e. in the form $(1-\beta)(\sigma_{SE}-\sigma_{ESA})$ for ESA in the $^4I_{13/2}$ level and $\beta(\sigma_{SE}-\sigma_{ESA})$ for ESA in the $^4I_{11/2}$ level. If we assume that pumping in any level above $^4I_{11/2}$ has the same effect on the above defined population ratio, comparisons can be made by using our β values, which is the purpose of the following discussion.

For the experiments performed with our Er^{3+}(4.75%):$LiYF_4$ sample under pumping with an Ar^+ ion laser excitation, comparison can be made with the results obtained with a sample of Er^{3+}(5%):$LiYF_4$ excited by a Kr^+ ion laser (647 nm) [11, 29], or with a Ti:Sa laser (~970 nm) [13]. Thus, by using the population ratio $\beta = 0.46$ found in our experiments (table 4) these results were found to agree with ours to better than 40%, which is quite satisfactory.

For the experiments made with our Er^{3+}(1.07%):$LiYF_4$ sample under Ar^+ ion laser pumping, comparison can be made in turn with the results obtained with an Er^{3+}(1%):$LiYF_4$ sample under the same pumping conditions [30]. With an estimated population ratio $\beta = 0.27$ (table 4) the results again agree satisfactorily, except around 800 nm where our ESA cross sections from the $^4I_{13/2}$ and $^4I_{11/2}$ levels are about half those deduced from the literature data, and around 1.5 μm, a wavelength domain for which we are very confident in our results because of the quality of the spectra and the good agreement found between the experimental integrated ESA cross sections and those derived from the JO calculations.

3.3.2. $^4S_{3/2}$ emission domains. The $^4S_{3/2}$ energy level of Er^{3+} in $LiYF_4$ leads to three types of laser emission: in the green at 551 nm (transition $^4S_{3/2} \rightarrow {}^4I_{15/2}$) [7] and in the near infrared at 850 nm (transition $^4S_{3/2} \rightarrow {}^4I_{13/2}$) [30] and 1.73 μm (transition $^4S_{3/2} \rightarrow {}^4I_{9/2}$) [31]. According to figure 6, laser emission at 850 nm falls in the tail of the $^4I_{13/2} \rightarrow {}^4S_{3/2}$ ESA band and laser emission at 1.73 μm is not affected by the $^4I_{13/2} \rightarrow {}^4I_{9/2}$ ESA transition (figure 4). According to figure 9, there is a weak ESA at 551 nm, which can be assigned to a $^4I_{11/2} \rightarrow {}^4G_{7/2}$ transition, with a cross section not exceeding about 2×10^{-21} cm^2. This is not negligible but it is clearly much weaker than the high cross section of about 2.1×10^{-20} cm^2 which characterizes [23] this emission transition.

These various $^4S_{3/2}$ laser emissions can be obtained by using direct [7] and upconversion processes excitation schemes. Upconversion can be obtained in two ways.

The first one is the result of two-step excitation via level $^4I_{9/2}$ around 810 nm or level $^4I_{11/2}$ around 970 nm [8, 9] (figure 1). In this case, our ESA spectra reported in figures 5 and 6 have particular interest. They confirm the results given in [13]. With our cross section spectra it is possible to determine the optimal wavelengths for two-step upconversion pumping. Around 970 nm, there are two GSA peaks at 969.2 and 971.7 nm, and three ESA peaks at 965.9, 972 and 973.8 nm. A maximum overlap between ESA and GSA is thus obtained around 972 nm

with $\sigma_{GSA} = 1.2 \times 10^{-20}$ cm^2 and $\sigma_{ESA} = 1.9 \times 10^{-20}$ cm^2, though the 973.8 nm region is also interesting with $\sigma_{GSA} = 0.3 \times 10^{-20}$ cm^2 and $\sigma_{ESA} = 2.1 \times 10^{-20}$ cm^2. In the 810 nm domain, there is an ESA peak at 811.3 nm with $\sigma_{ESA} = 1.0 \times 10^{-20}$ cm^2, which corresponds to a GSA with a 0.4×10^{-21} cm^2 cross section. There is also an ESA peak at 790.8 nm with $\sigma_{ESA} = 0.5 \times 10^{-20}$ cm^2, which is associated with a $^4I_{13/2} \rightarrow {}^4H_{11/2}$ transition, which is useful to depopulate the terminal level of the laser $^4S_{3/2} \rightarrow {}^4I_{13/2}$ at 850 nm [30]. This wavelength excitation, with an ESA cross section half that at 811.3 nm, could serve for the 551 nm laser emission, because GSA at 790.8 nm ($\sigma_{GSA} = 0.8.10^{-21}$ cm^2) is twice that at 811.3 nm. In one laser experiment [27], the beams of two laser diodes were combined by a polarization beam splitter to increase the pump power. The anti-Stokes pump efficiency could be improved by using two diodes at different wavelengths: one emitting at the maximum GSA peak in σ polarization and the second emitting at the maximum ESA peak in π polarization at 965.9 nm.

The second anti-Stokes excitation method can be obtained by photon avalanche upconversion. The avalanche process was observed at room temperature with Er^{3+}:$LiYF_4$, among others, by Auzel and Chen [10] and their study demonstrated the usefulness of ESA from the $^4I_{11/2}$ level around 579 and 690 nm but also of ESA from the $^4I_{13/2}$ level around 707 nm. Our ESA results completely agree with these findings and allows us to give all the ESA cross sections at the various pump wavelengths (579.6 nm: 1.5×10^{-20} cm^2; 688.8 nm: 0.6×10^{-20} cm^2; 707.9 nm 1.4×10^{-20} cm^2) which are necessary to understand and simulate the observed avalanche effect.

In the end, it is worth noting that energy transfer (figure 1) strongly influence the energy level populations, thus photon avalanche upconversion and 2.8 μm laser emission, for example. These energy transfers are described microscopically by microparameters which are proportional to the overlap integrals of the GSA and ESA cross sections implied in the transfers [32]. For the $^4I_{13/2}$, $^4I_{13/2} \rightarrow {}^4I_{9/2}$, $^4I_{15/2}$ upconversion energy transfers around 1.6 μm (see figure 4), the overlap is weak, which corresponds to an energy transfer microparameter value of about 10^{-48} cm^5, when a much greater value of 3.4×10^{-47} cm^5 (in π polarization) is found for the $^4I_{11/2}$, $^4I_{11/2} \rightarrow {}^4F_{7/2}(^4S_{3/2})$, $^4I_{15/2}$ energy transfers around 970 nm. For the highly doped crystals, however, energy transfers are combinations of direct donor–acceptor and donor–donor migration assisted energy transfers [32]. Then, overlap integrals of GSA and SE cross sections must be further considered. Doing so, we realize that the overlap integrals corresponding to the migration type energy transfers $^4I_{13/2}$, $^4I_{15/2} \rightarrow {}^4I_{15/2}$, $^4I_{13/2}$ and $^4I_{11/2}$, $^4I_{15/2} \rightarrow {}^4I_{15/2}$, $^4I_{11/2}$ give values of 30×10^{-47} cm^5 and 5×10^{-47} cm^5, respectively. Thus, level $^4I_{11/2}$ should be less affected than level $^4I_{13/2}$ by migration. Consequently, in the case of the highly concentrated crystals suitable for 2.8 μm laser operation, for which the population ratio β remains close to 0.45 whatever the excitation pump wavelength (table 4), the overall efficiencies of the energy transfers in the $^4I_{11/2}$ and $^4I_{13/2}$ levels should be very similar.

4. Conclusion

We have shown that it is possible to estimate ESA cross sections from different metastable states, provided that their population ratio is measured in appropriate conditions. This technique has been applied here to the Er^{3+}:$LiYF_4$ system and a general good agreement has been found between our results and those which can be deduced from the past literature. In the course of the measurements, we have measured for the first time the β_{Rad}/τ_{Rad} ratio for the 2.8 μm laser transition $^4I_{11/2} \rightarrow {}^4I_{13/2}$, the obtained value of 20 s^{-1} being in good agreement with the prediction made by using the Judd–Ofelt (JO) formalism. The experimentally derived integrated cross section of this 2.8 μm laser transition and that for other important laser transitions such as the green one at 551 nm also agree well with the results of this JO

analysis. The gain cross sections for the 2.8 μm laser transition are obtained for different Er^{3+} concentrations and pumping wavelengths. The highest population inversion, close to 0.5, is obtained for the 14.75 at.% Er^{3+} doped crystal, whatever the pumping wavelength. It is thus demonstrated that 2.8 μm CW laser operation is possible by pumping around 1.51 μm in the terminal level of the laser transition, in good agreement with past and recent observations [4, 28].

We have also measured the cross sections of the ESA transitions which can be involved, either in a two-step absorption or a photon avalanche process, in order to obtain the characteristic green emission of Er:$LiYF_4$ and the results nicely complete the relative ESA cross section measurements of the literature.

References

[1] Kintz G J, Allen R and Esterowitz L 1987 *Appl. Phys. Lett.* **50** 1553
[2] Frauchiger J and Luthy W 1987 *Opt. Quantum Electron* **19** 231
[3] Barnes N P 1995 *Laser Focus World* April 87
[4] Xie P and Rand S C 1990 *Opt. Lett.* **15** 848
[5] Stoneman R C, Lynn J G and Esterowitz L 1992 *IEEE J. Quantum Electron.* **28** 1041
[6] Auzel F, Hubert S and Meichenin D 1989 *Appl. Phys. Lett.* **54** 681
[7] Brede R, Danger T, Heumann E, Huber G and Chai B 1993 *Appl. Phys. Lett.* **63** 729
[8] Heine F, Heumann E, Danger T, Schweizer T, Huber G and Chai B 1994 *Appl. Phys. Lett.* **65** 383
[9] Heine F, Heumann E, Möbert P, Huber G and Chai B H T 1995 *OSA Proc. ASSL* **24** 74
[10] Auzel F and Chen Y 1995 *J. Lumin.* **65** 45
[11] Koetke J and Huber G 1995 *Appl. Phys.* B **61** 151
[12] Le Boulanger P, Doualan J-L, Girard S, Margerie J and Moncorgé R 1999 *Phys. Rev.* B **60** 11 380
[13] Pollnau M, Lüthy W, Weber H P, Krämer K, Güdel H U and McFarlane R A 1996 *Appl. Phys.* B **62** 339
[14] Aull B F and Jenssen H P 1982 *IEEE J. Quantum Electron.* **18** 925
[15] McCumber D E 1964 *Phys. Rev.* **136** A954
[16] Couto Dos Santo M A, Antic-Fidancev E, Gesland J Y, Krupa J C, Lemaître-Blaise M and Porcher P 1998 *J. Alloys Compounds* **275–277** 435
[17] Judd B R 1962 *Phys. Rev.* **127** 750
[18] Ofelt G S 1962 *J. Phys. Chem.* **37** 511
[19] Li C, Guyot Y, Linarès C, Moncorgé R and Joubert M F 1993 *OSA Proc. ASSL* **15** 91
[20] Li C 1992 Spectroscopie, dynamique de fluorescence et potentialité laser des cristaux Y_2SiO_5:Er^{3+}, Y_2SiO_5:Yb^{3+}, Er^{3+} et Y_2SiO_5:Tm^{3+} *Thesis*
[21] Tkachuk A M, Poletimova A V and Petrov M V 1985 *Opt. Spectrosc.* **59** 680
[22] Hubert S, Meichenin D, Zhou B W and Auzel F 1991 *J. Lumin.* **50** 7
[23] Wyss C, Luthy W, Weber H P, Rogin P and Hulliger J 1997 *Opt. Commun.* **139** 215
[24] Diening A, Jensen T and Huber G 1996 *EQEC: OSA Tech. Digest Ser.* **110**
[25] Knowles K and Jenssen H P 1992 *IEEE J. Quantum Electron.* **28** 1197
[26] Pollnau M, Graf Th, Balmer J E, Luthy W and Weber H P 1994 *Phys. Rev.* A **49** 3990
[27] Jensen T, Diening A, Huber G and Chai B H T 1996 *Opt. Lett.* **21** 585
[28] Labbe C, Doualan J L, Girard S, Moncorgé R and Thuau M 1999 *Proc. Int. Conf. on Lasers '98* ed V J Corcoran and T A Goldman pp 217–220
[29] Danger T, Koetke J, Brede R, Heumann E, Huber G and Chai B H T 1994 *J. Appl. Phys.* **76** 1413
[30] Möbert P E-A, Heumann E, Petermann K, Huber G and Chai B H T 1998 *Tech. Digest ASSL 98* AMA2
[31] Barnes N P, Allen R E, Esterowitz L, Chicklis E P, Knights M G and Jenssen H P 1986 *IEEE J. Quantum Electron.* **22** 337
[32] Caird J A, Ramponi A J and Staver P R 1991 *J. Opt. Soc. Am.* B **8** 1391